10.48047/jocaaa.2022.30.02.78

Optimization of Micro Plasma Welding Parameters for SS310 Butt Joints: A Response Surface Methodology Approach

Harish Kumar Arya
SantLongowal Institute of Engineering and Technology,
Longowal, Punjab, India
ORCID Id: 0000-0001-8074-3477b, 0000-0002-0709-4148f
Deepti Jaiswal
Indira Gandhi Delhi Technological University, Delhi, India;
ORCID Id:0009-0009-5898-8641
***Corresponding Author: arya.iitr@gmail.com**

Abstract:

This journal article is a detailed study of the micro plasma welding of SS310 welding material to butt joint using a 500 μm thick material. The main aim of the study is to examine the effects of three important parameters in welding, namely, welding speed, current and standoff distance (SOD) on a systematic basis but at three different levels each. Using Response Surface Methodology (RSM), 20 sets of welding parameters were produced and carefully tested to determine their effect on the successful development of butt joints in SS310.

The performance of the weld joint was evaluated using a multifaceted method that entailed tensile tests, micro-hardness, and the metallographic analysis. These techniques offered useful answers regarding the mechanical characteristics and microstructure of the welded joints that allowed to assess the quality of welding holistically.

The best process parameters were determined through rigorous analysis to come up with high quality welds in SS310 with the recommended ranges of welding speed of 2-4 mm/s, current of 5-7.5 amps and standoff distance of 2-4 mm was found to predict the micro-hardness and tensile strength mathematically and thus it could be seen that the mathematical models agreed with the validation results.

10.48047/jocaaa.2022.30.02.78

Introduction

RSM or Response Surface Methodology is a set of mathematical and statistical methods that is used to analyse a situation in which a dependent variable or response is affected by a number of independent variables. The main goal of RSM is to optimize the response variable in such situations. When dealing with Response Surface Methodology (RSM), the particular association among the response variable and the independent variables is not known in most instances. Therefore, identifying a proper approximation of the actual functional relationship between the response and the collection of independent variables is the first step in RSM. A low-order of a polynomial is normally used to represent the relationship in a certain area of the independent variables. When the response is sufficiently described by a linear equation of the independent variables, then a first-order model is used. But in case the system is curved, a higher-degree, say a second-order model, is taken. RSM is a step-by-step process which seeks to find the best possible operating conditions of the system or a region in the factor space where the desired operating specifications are achieved.

plasma welding is a flexible and is used in a variety of joining processes, such as miniature component welding, seam welding, and large scale production welding among others. The principle of the plasma arc welding (PAW) process is the same as that of gas tungsten arc welding (GTAW) in that the heat is produced by the arc to weld the joint and filler metal is added when needed to form [2]. Micro-Plasma arc welding (PAW) is widely known to have a better concentration of energy when compared to the GTAW process which has superior characteristics of deeper penetration, arc stability and precision of the process [3]. Microplasma welding is a process that requires specialized welding and has to be operated by skilled people. It demands skills in the manipulation of the microplasma torch, the welding parameters and constant arc stability [4]. micro plasma processing in

10.48047/jocaaa.2022.30.02.78

microscale welding has unique benefits over GTAW. It is however notable that little has been done to investigate the micro plasma arc welding (MPAW) process as such in the currently available literature although the process has many benefits [5]. The nickel content in the stainless-steel structure makes the austenitic phase to be stabilized even at room temperature[6]. It is a cost-effective structural material that is known to have excellent resistance to corrosion, is easy to weld, and has excellent mechanical properties [7]. It is normally used in various fields such as petrochemical, chemical, offshore structures, structural engineering, nuclear reactors, as well as biomedical where it is used as an implant material [8]. As a result of these wide range of application areas, austenitic stainless steels (ASSs) take about 70 percent of the total stainless-steel usage [9].

Austenitic stainless steels (ASSs) have a moderate amount of ductility and may undergo significant contraction yet they are prone to cracking as they cool-down[10]. Problems created by weld joints in austenitic stainless steels (ASSs) become more complicated when carbides develop within the grain boundary (GB), and eventually lead to sensitization and weld decay[11]. To optimize the process parameters, researchers have employed Taguchi orthogonal array, regression models and ANOVA methods [12]. ANOVA analysis revealed significant factors and interactions and scatter plots proved that the models were accurate in predicting the weld bead geometry parameters such as the effect of input parameters on the front and back width [13]. Plasma arc welding (PAW) has greater arc control with reduced levels of welding current and reduced heat-affected areas compared to the conventional arc welding methods [14]. The geometry of the weld beads is especially influenced by the changes in the welding current and speed of the welding process[15].When a very low electrical current is passed through a small orifice the resulting jet of plasma is a needle plasma jet. This slender, pointed arc that is created between 0.1 and 15 A currents is an effective deterrent to arc drift. By contrast, the gas

10.48047/jocaaa.2022.30.02.78

tungsten arc at similar currents is unstable and has a drifted arc and is not as focused. Compared to the other types of micro-plasma jets, the micro-plasma jet provides better control and stability at low currents, decreased sensitivity to arc length changes, and is capable of varying arc length considerably (up to 20 mm) without onset of instability or excessive spreading of the arc [16-18]. In low-current foil welding applications, the process features and operational parameters that can impact weld appearance and quality become particularly crucial[19]. The material characteristics are highly changed by the high amount of heat passed through the weld bead[20]. Scientists have come up with a mathematical representation of determining the temperature distribution and the results of the simulation are in good agreement with the experimental data[21]. The use of numerical modeling is crucial in modeling temperature profiles, although effective numerical models that are specifically developed to suit micro-scale welding processes are limited[22]. Thermo-mechanical studies, which can be conducted with the help of experimental research and 3D finite element modeling, can provide more reliable results in terms of the required amount of heat input, heat-affected zones (HAZ), distortion, and changes in the mechanical and microstructural properties of thin austenitic stainless-steel sheets [23]. Simulations and experimental validation have been done by the researchers to explore the effect of the deposition direction on temperature and temperature gradient[24].

Material and Method

The permanent joining of SS310 with 500 μm thickness is selected in the μ-PAW process. The chemical composition of SS310 is presented in table 1.

Table 1 Chemical composition of SS310 (wt. %).

10.48047/jocaaa.2022.30.02.78

Elements	C	Cr	Mn	Ni	P	S	Si	Fe
Wt. (%)	0.047	24.52	1.24	19.18	0.027	0.01	0.322	Balance

The experiments were carried out using a micro plasma arc welding machine with DC power supply between 0.5 A and 120 A. An adapted system was designed, which consisted of a welding manipulator, and a table with a welding torch, and weld plates attached to it. The torch was connected to an assembly which could make it move in a straight line using a stepper motor. This manipulator was working with a lead screw which was driven by another stepper motor. A computer with an Arduino program was used to control the stepper motor making it adjust its rpm. As a result, the linear motion was converted into the rotational motion of the lead screw using the welding manipulator, where there was the welding torch.

In the initial experiments, the dimensions of sheets cut by Leg Shearing Machine were 100x50x 0.5 mm to ensure that the welding of the SS310 sheets was successful. These experiments entailed controlled variations of the welding conditions under the same conditions of some factors held constant. The important variables were the welding current, speed and stand-off distance (SOD). The welding speed determination process started with a minimum welding setting and was fine-tuned. The discovery of a constant welding current, which is important in obtaining sound joints, was realized through intensive experiment. The best welding speed ranging was above 2 mm/s and the range of welding current was 5 A to 8 A to avoid burning materials. Maintaining a constant welding current and speed and systematically changing the distance formed the basis of establishing the SOD. It was found that below 2mm SOD, there were problems with burn-through or unstable arcs and above 4mm, there was a lower heat input leading to shallow penetration and increased width of the welds. Successful parameters criteria were set in

10.48047/jocaaa.2022.30.02.78

terms of perfect appearances and the lack of flaws. This procedure resulted in the selection of a given parameter range, as shown in the table 2, to have effective SS310 welding joints.

Table 2 Parameters selected after conducting trial runs.

Parameters	Welding Current (A)	Welding Speed (mm/s)	SOD (mm)
Range	5 - 7.5	2 – 4	2 - 4

The first stage is to make sure that the edges of the pieces to be joined are properly prepared, then to wash them with acetone to eliminate any trace of oil, dirt or grease and then left to dry thoroughly. The pieces are carefully positioned so as to leave no loopholes. The base metal plates are tacked to ensure that the same distance is maintained throughout the length of the joint, and that there are no deformations that may affect the final outcome. Arguon gas is used to start the arc which not only forms the arc, but also protects the welding area against impurities in the atmosphere. A copper fixure is precisely designed to firmly fix the workpieces. This fastener has two very important functions, (i) to provide a good fit of the pieces, and (ii) to utilize the good conductive nature of copper to conduct away heat produced during the joining process so that distortion in thin sheets does not occur. Thermocouples, and a data logger are used to measure the temperature distribution on the plates throughout the welding process. These thermocouples are spaced on different points on the sheet to ascertain the temperature distribution during MPAW process.

10.48047/jocaaa.2022.30.02.78

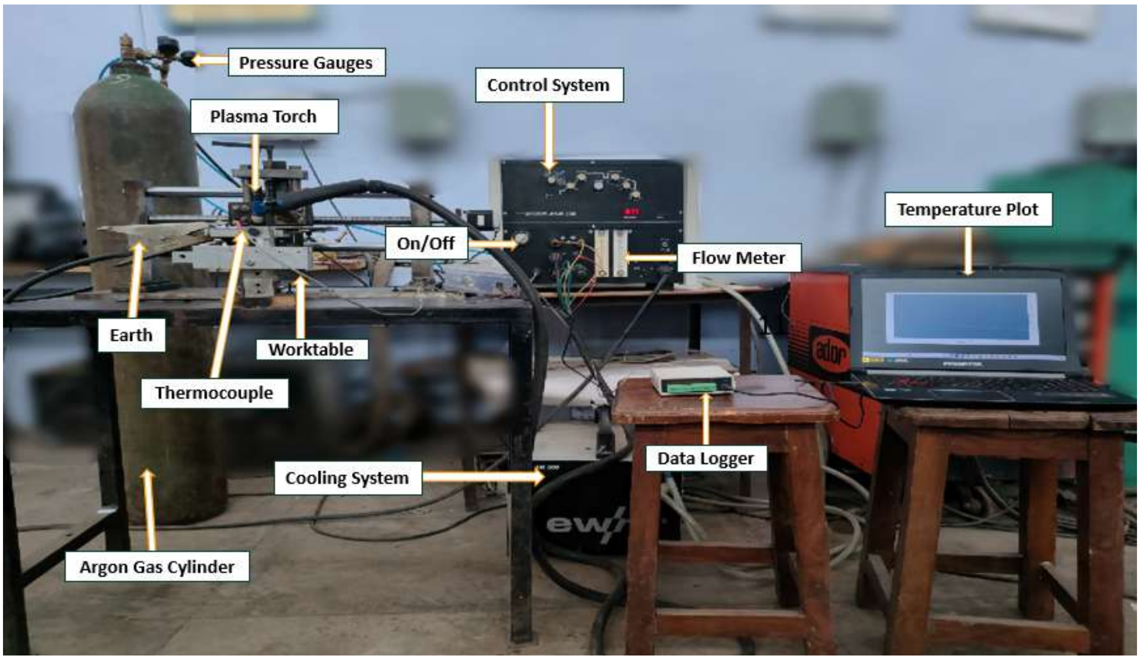

Figure 1 Experimental layout employed for the present investigation.

Face-centred center composite design (CCD) was selected as the experimental design of this study, after analysing the factors carefully and the data needed to conduct the study. Response Surface Methodology (RSM) was used to determine the effect of three independent process variables including: welding current, stand-off distance and welding speed, all of which had three levels. The middle levels of these variables were taken as the middle points whereas the integration of each of the variables at the lowest level (-1) or the highest level +1 with the rest two variables at the intermediate level formed the star points. Through 20 experiments we performed, under varying circumstances, we were able to estimate not only the linear but also the quadratic effect of these parameters on the properties of the welded joints. The choice of the parameter ranges and combinations was based on the following criteria: machine capabilities, the plan to obtain visually appealing, defect-free welds and the appropriate layout of welds.

10.48047/jocaaa.2022.30.02.78

Table 3 Welding parameters and their levels.

Parameter	Notation	Units	Levels		
			-1	0	+1
Welding current	I	A	5	6.25	7.5
Welding speed	V	mm/sec	2	3	4
Standoff distance	SOD	mm	2	3	4

The welding of SS310 sheets was done using the given set of 20 parameters. It was a micro plasma machine provided by EWM with current range of 0.1A to 120A, which was varied according to the thickness of the sheet. Fine tungsten electrode was used in the welding process, which involved using of argon as the shielding and plasma gas, and a DCEN polarity at 25 V.The further details can be found in the table.

Table 4 Conditions for welding.

Power supply	EWM micro plasma machine
Polarity	DCEN
Operation mode	Non-pulse operation
Electrode	(2%) thoriated tungsten electrode
Diameter of electrode	1 mm
Plasma gas	Argon
Shielding gas	Argon
Flow rate of shielding gas	6Lpm
Flow rate of plasma gas	0.6Lpm
Copper Nozzle diameter	1 mm
Torch position	Vertical

10.48047/jocaaa.2022.30.02.78

Operation type	Automatic

The weld joints were then prepared according to the design matrix and then, both mechanical and metallurgical tests were carried out on test specimens taken out of the weld joints. In particular, two tensile test specimens, one microhardness test specimen, one metallography sample and one bend test specimen were carefully prepared out of each joint. The sample plan for evaluating the weld joints' mechanical and metallurgical properties is illustrated in Figure 2.

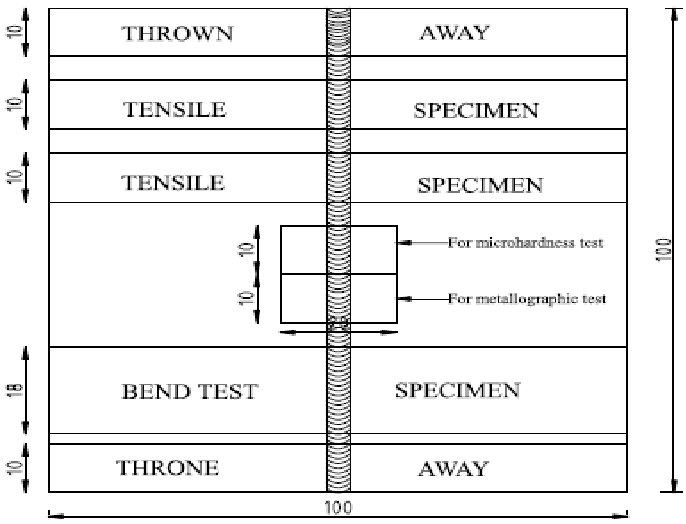

Figure 2 Weld sample plan for metallographic analysis and mechanical testing.

Mechanical properties of weld joint

The ASTM specifications, namely, E-8M-04 [ASTM-2008], were used to prepare test samples of transverse tensile testing, which were the weld joint. CNC wire cut EDM (Electrical Discharge Machining) was used in preparing the test samples. There are two tensile specimens which are prepared in each welding condition and the average is taken

10.48047/jocaaa.2022.30.02.78

into account here. The test was carried out at a constant rate of 0.5 mm/min [26]. This was tested on Universal Testing Machine in Welding Metallurgy Lab, SLIET Longowal.

Figure 3 : Some tensile test specimens.

Metallurgical examination

To have a closer look at the weld structure, the samples were cut out of the weld in transverse direction. A 20 x 10 mm piece was cut out of the welded sheets both parallel and perpendicular to the weld. These samples were then polished with varying finer polishing papers, the grit size of 100-3000After polishing, the samples were then electro-etched to make the microstructure more visible. Electro etchant is made of 80% ethanol and 20% perchloric acid. Electro etching of the specimen was then done by placing the specimen in the etchant that had been prepared by Carpenter, 20 sec. Acids in the etchant used attacked the boundaries of the grains giving a clear picture of the grain structures. The samples were then etched and properly washed to clear out the carbon deposits and then dried before viewing under optical microscope to study the microstructure.

Table 5 Carpenter's etchant constituents.

Constituents	Quantity

10.48047/jocaaa.2022.30.02.78

$FeCl_3$	8.5 g
$CuCl_2$	2.4 g
HCL	122 ml
HNO_3	6 ml
Ethanol	122 ml

Microhardness survey

Microhardness of weld and heat affected areas was researched through the OMNITECH Microhardness Tester at the SLIET Longowal. The etching was done using specimens to examine different areas of weldment and measurements were made at 1 mm intervals along the centerline of the weld. The pyramid diamond indenter of a Vickers was used to test the MVH-II tester, which applied a 500 gm load within 20 seconds. Results showed variations in microhardness in the weld, heat-affected and base metal areas, which allowed the overall interpretation of the mechanical properties of the material within the weld, heat-affected and base metal areas.

10.48047/jocaaa.2022.30.02.78

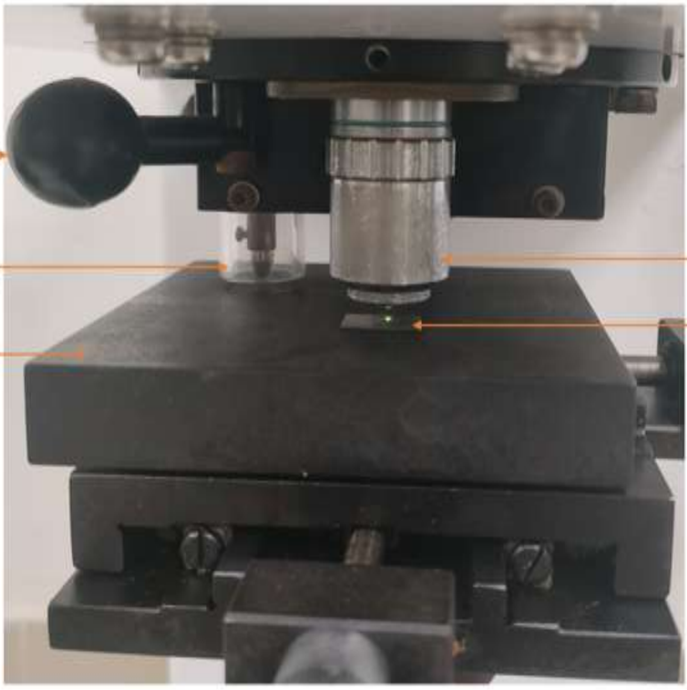

Figure 4 Vickers microhardness worktable.

Result & Discussions

The number of experiments carried out was 20 based on the design matrix with three process parameters at three levels. All these experiments were carried out in accordance with the test conditions outlined in the second-order central composite design. Table 6 shows the experimental values of tensile strength and microhardness results.

Table 6 Design matrix and experimental results.

	Factor 1	Factor 2	Factor 3	Response 1	Response 2
Run	A:CURRENT	B:Speed	C:SOD	TENSILE STRENGTH	MICROHARDNESS

10.48047/jocaaa.2022.30.02.78

	Ampere	mm/sec	Mm	MPa	Hv
1	6.25	3	3	526	190.87
2	5	4	4	506	150.25
3	5	2	4	498	160.37
4	6.25	3	3	525	191.14
5	6.25	3	2	517	186.46
6	6.25	3	3	526.5	191.87
7	6.25	3	4	519	180.15
8	7.5	3	3	513	182.14
9	5	3	3	521	180.02
10	7.5	4	2	494	160.25
11	7.5	2	2	491	176.00
12	5	2	2	503	166.29
13	7.5	4	4	505	155.54
14	5	4	2	508	150.12
15	6.25	3	3	527.5	191.85
16	7.5	2	4	493	165.26
17	6.25	3	3	526	192.26
18	6.25	4	3	520	172.13
19	6.25	3	3	527	193.36
20	6.25	2	3	512	185.25

Regression analysis was used to develop mathematical models using experimental data. The effect of the welding parameters; current (I), standoff distance (SOD), and speed (V) on the weld joints was predicted in these models of the linear and quadratic effects. They

10.48047/jocaaa.2022.30.02.78

accurately forecasted tensile strength and microhardness. Response surface methodology was also used to measure the effects of interaction.

Mathematical model selection

The micro plasma arc welded joints response (Y) is related to the current applied in the welding (I), standoff distance (D) and the welding speed (V). It could be stated as follows:

$$Y = f(I, D, V) \quad (2)$$

A second-order regression equation of the form of a second order seem to represent the response surface Y.

$$Y = b_0 + \Sigma b_i x_i + \Sigma b_{ii} x_i^2 + \Sigma b_{ij} x_i x_j + e \quad (3)$$

The regression equation is a combination of separate terms. The fixed value 'b0' represents the mean of the response. The representations of bi, bii, bij, and e are linearity, interaction, quadratic and residual error respectively. The parameter interactions can be seen in the coefficients such as b0, bi, bii and bij which are least-squares estimates of the polynomial. These parameters are known as response function parameters and they illustrate the results of trials prepared with the help of DESIGN EXPERT and analysed statistically in the same program. The selected poly can be expressed as below in four factors,

$$Y = b_0 + b_1(I) + b_2(V) + b_3(D) + b_{12}(IV) + b_{13}(ID) + b_{23}(VD) + b_{11}(I^2)$$

$$+ b_{22}(V^2) + b_{33}(D^2) \quad (4)$$

Mathematical model for tensile strength

10.48047/jocaaa.2022.30.02.78

To identify whether the developed model was adequate, the analysis of variance (ANOVA) method was utilized whereby the estimated Fratio of the generated model should be less than the standard Fratio (as shown in the F-table) value at a selected degree of confidence.

Table 7 Model developed for Tensile strength

Source	Sum of Squares	df	Mean Square	F-value	p-value	Remarks
Model	2903.78	9	322.64	276.46	0.0001	significant
I-CURRENT	168.10	1	168.10	144.04	0.0001	
V-speed	122.50	1	122.50	104.97	0.0032	
D-SOD	8.10	1	8.10	6.94	0.0020	
IV	1.12	1	1.12	0.9640	0.3493	
ID	45.12	1	45.12	38.67	0.0001	
VD	15.12	1	15.12	12.96	0.0048	
I^2	211.64	1	211.64	181.35	0.0001	
V^2	262.64	1	262.64	225.05	0.0001	
D^2	166.14	1	166.14	142.36	0.0001	
Residual	11.67	10	1.17			
Lack of Fit	7.84	5	1.57	2.04	0.2256	not significant
Pure Error	3.83	5	0.7667			
Cor Total	2915.45	19				

R^2 = 99.67 %	**R^2(adjst.) = 99.37 %**	**R^2 (pred) = 96.00 %**

Tensile Strength = 526.13 - (I) 4 + (V) 3.60 + (D) 0.80 + (ID) 2.5 + (VD) 1.5 - (I^2) 8.82 - (V^2) 9.82 - (D^2) 7.82 (5)

- The Design Expert software was used to calculate the coefficients and the significance of the coefficients was evaluated at 99.67% using F-test.

10.48047/jocaaa.2022.30.02.78

- When p-value is lower than 0.0500, we can conclude that model terms are significant. Here, the terms I. V. D, IV, I^2, V^2, and D^2 could be identified as important.

- P-values above 0.1000 on the other hand are used to signify that the model terms are not significant. As a result, any terms with p-values more than 0.1000 were dropped out of the equation.

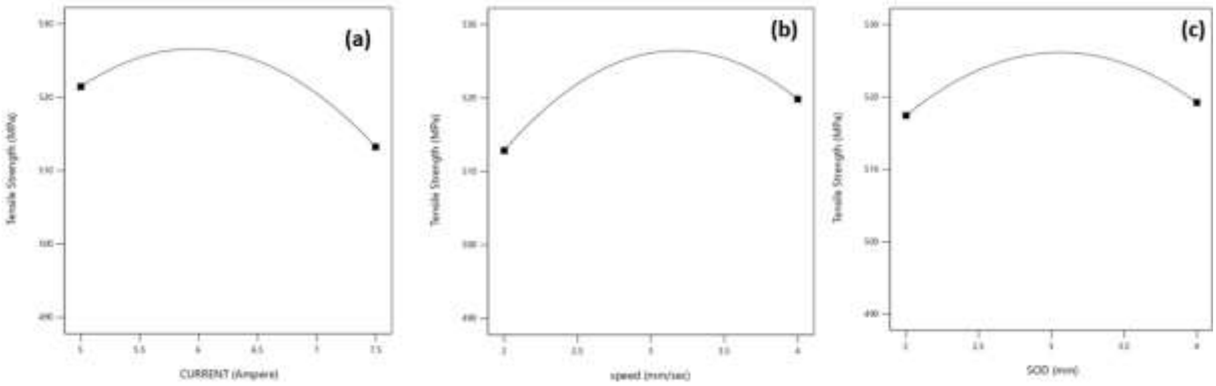

Figure 5 a) Effect of current, (b) Effect of speed, (c) Effect of SOD over Tensile strength.

10.48047/jocaaa.2022.30.02.78

Table 8 Model developed for Microhardness

Source	Sum of Squares	df	Mean Square	F-value	p-value	
Model	4232.43	9	470.27	390.31	0.0001	significant
I-CURRENT	150.30	1	150.30	124.74	0.0001	
V-speed	454.52	1	454.52	377.24	0.0001	
D-SOD	90.71	1	90.71	75.29	0.0001	
IV	0.4086	1	0.4086	0.3391	0.5732	
ID	18.88	1	18.88	15.67	0.0027	
VD	26.83	1	26.83	22.27	0.0008	
I^2	365.11	1	365.11	303.03	0.0001	
V^2	390.37	1	390.37	324.00	0.0001	
D^2	146.64	1	146.64	121.71	0.0001	
Residual	12.05	10	1.20			
Lack of Fit	8.15	5	1.63	2.09	0.2186	not significant
Pure Error	3.90	5	0.7793			
Cor Total	4244.48	19				

R^2 = 99.72 %	**R^2(adjst.) = 99.46 %**	**R^2 (pred) = 98.54 %**

Microhardness = 191.38 + (I) 3.88 - (V) 6.74 - (D) 3.01 - (ID) 1.54 + (VD) 1.83 - (I^2) 11.52

– (V^2) 11.91 - (D^2) 7.30 (6)

10.48047/jocaaa.2022.30.02.78

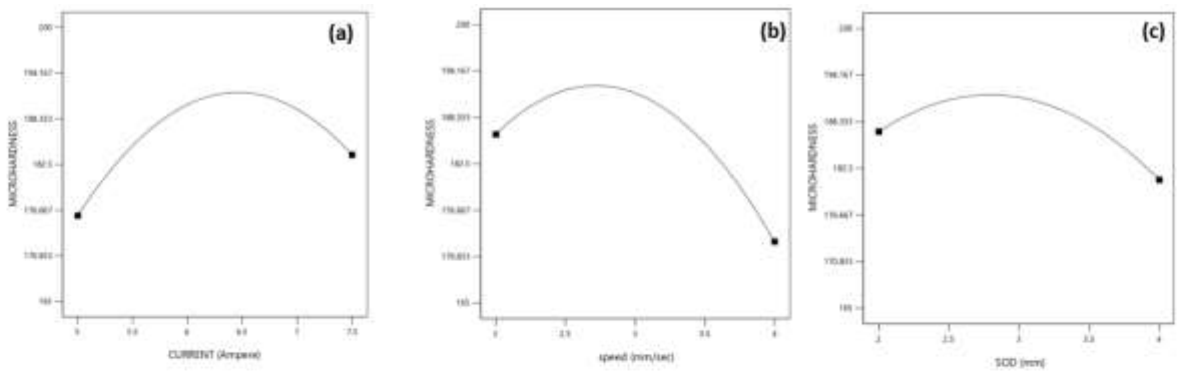

Figure 6 (a) Effect of current, (b) Effect of speed, (c) Effect of SOD over Microhardness.

Fig. 12, (a) Effect of current, (b) Effect of speed, (c) Effect of SOD over Microhardness.

Validation of models

In order to arrive at an optimum value of input parameters; welding current (I), welding speed (V), and standoff distance (SOD) we obtain maximum tensile strength and minimum microhardness and optimum values are presented in Table 10 below.

Table 9 Model validation and confirmation

Method	Process parameters	Responses

Microstructural studies of weld

	I (Amps)	V (Speed)	SOD (Standoff distance)	Tensile strength (MPa)	Microhardness (Hv)
Optimized	6.25	3	3	525	191.145
Validated	6.25	3	3	527.5	188.264
	Error			0.47%	1.50%

10.48047/jocaaa.2022.30.02.78

Microstructure is of great significance in welding processes and greatly influences properties and performance of the welded joints. Fig.7 shows the microstructure of SS 310 base metal.

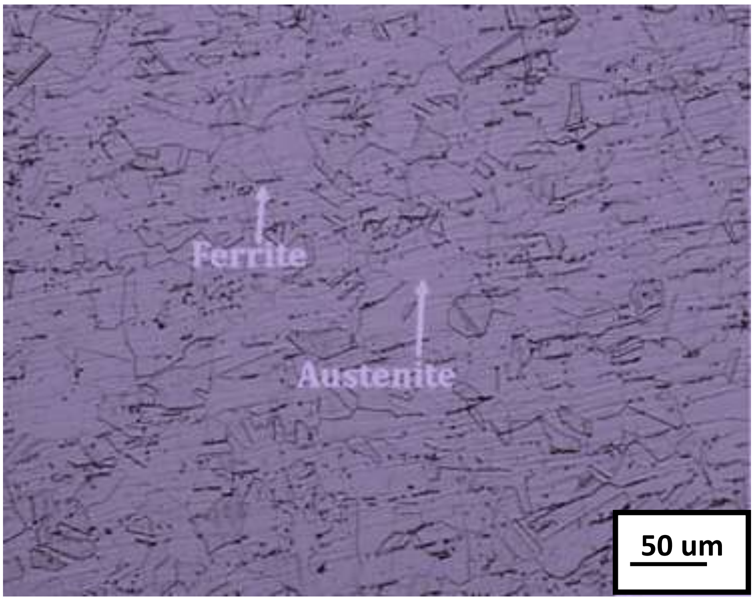

Figure 7 Microstructure of the SS 310 base metal in the as-received condition.

The SS 310 base metal image reveals the existence of the combination of austenitic, and ferritic phases. The isolation of the elements that promote the development of ferrite at the time of solidification of the material results in the occurrence of the ferrite phase in austenitic stainless steel.

10.48047/jocaaa.2022.30.02.78

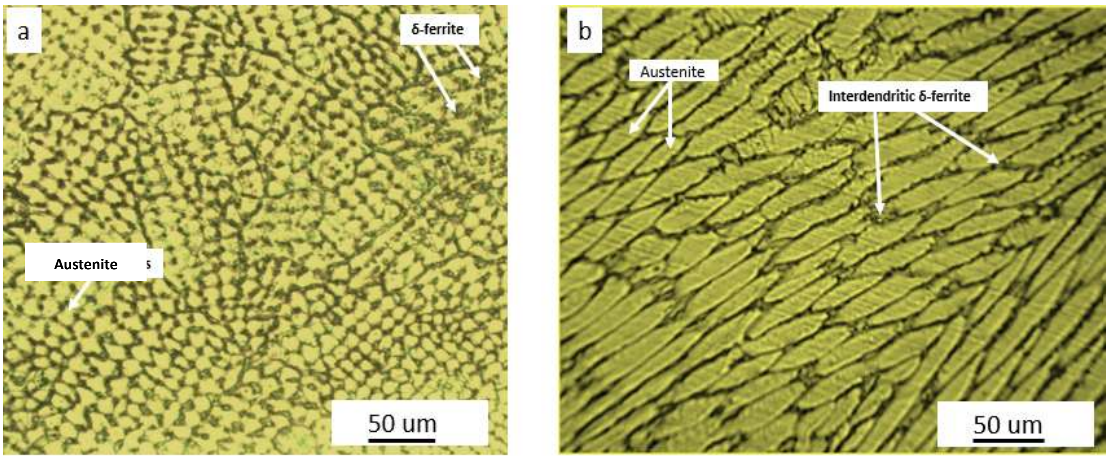

Figure 8 The microstructure of SS 310 (a) weld metal center in high cooling rate (b) weld metal center in low cooling rate.

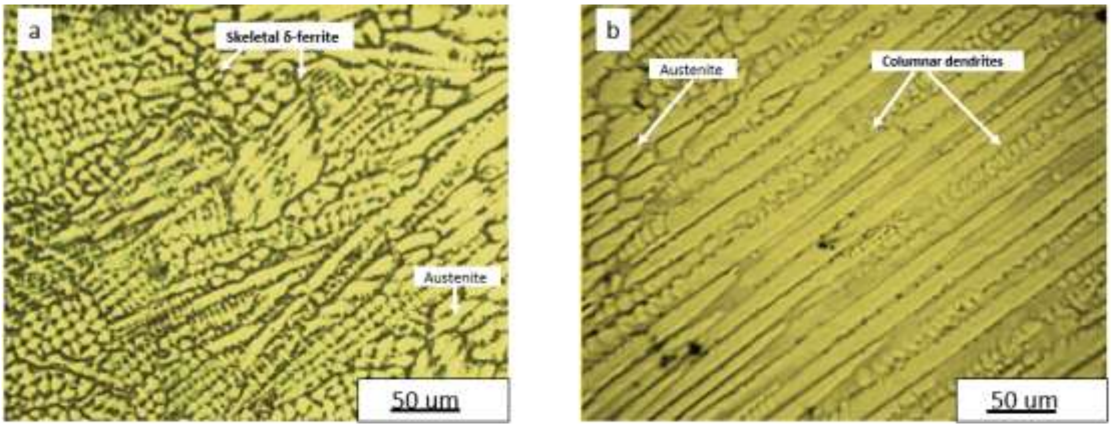

Figure 9 The microstructure of SS 310 (a) on either side of the fusion line at a high cooling rate, and (b) on either side of the fusion line at a low cooling rate.

The fine equiaxed grains observed in Fig. 8 (a) of SS 310 in the weld area could have been a result of the high cooling rate. The quicker cooling rate is more likely to develop smaller and evenly spaced grains. Alternatively, the δ-ferrite could be due to slower cooling within the Interdendritic regions, which has a relatively slower cooling rate.

However, the development of Interdendritic δ-ferrite grains in Fig. 8 (b) may be explained by the slower cooling rate as well as because the austenitic steels contain alloying elements, including chromium. Slower rate of cooling gives enough time to alloying elements such as chromium to separate and form clusters in the Interdendritic

10.48047/jocaaa.2022.30.02.78

areas. This addition of stabilizing elements in ferrite results in the formation of the δ-ferrite grains within such regions [26-27].

Fig. 9 (a) and Fig. 9 (b) show the microstructure in the vicinity of the fusion line region at various cooling rates. Both areas have austenite. Ferrite in Fig. 9 (a) could be explained by the high chromium-content in SS 310. Fig. 9 (b) suggests that the columnar dendrites predominating around the fusion lines are probably due to the slower rate of cooling which gives plenty of time to grow grains and convert them into columnar dendrites[28].

Higher cooling rates in weld joints results in a finer microstructure, overly rapid cooling should be avoided as it can result in brittle microstructures and possible cracking, which would have a negative impact on tensile strength.

Effect of cooling rate on microhardness

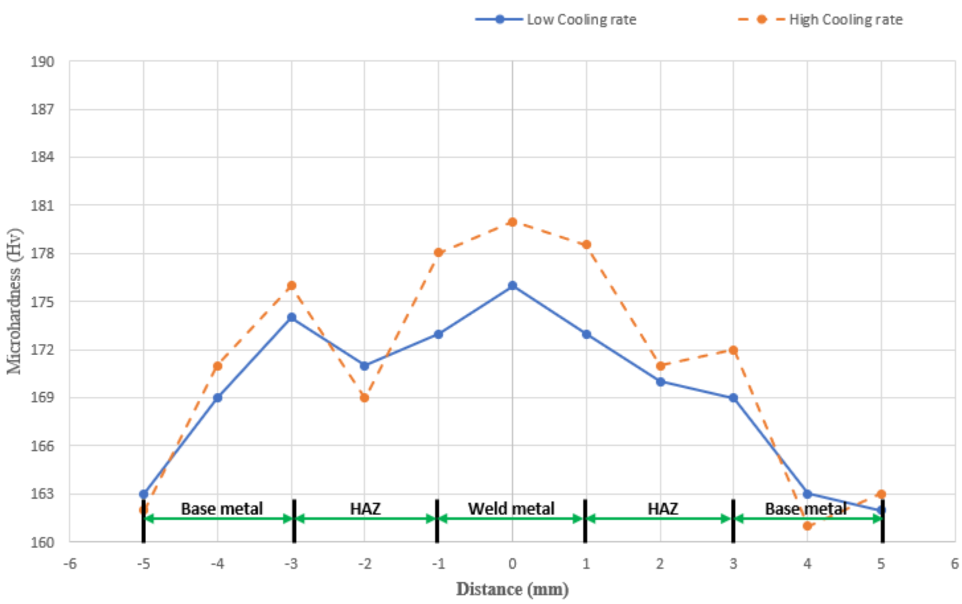

Figure 10 Change of micro hardness with the rate of cooling

10.48047/jocaaa.2022.30.02.78

Fig. 10 shows that the finer the microstructure, the greater the microhardness as the smaller the grains are and the slower is the rate of dislocation motion. This process can be accelerated by faster cooling as well contributing to increased hard phase and higher microhardness. On the other hand, reduced cooling rate forms a more coarse microstructure with less microhardness with the large grains being able to move dislocations easily to form a softer material [29].

Effect of cooling rate on tensile strength

With austenitic stainless steels, high cooling rates provide a more refined microstructure with smaller grains which increases tensile strength by preventing the freezing of dislocations. The high cooling rate can also assist in formation of hard phases which will enhance tensile strength. On the other hand, low cooling rates produce a coarser microstructure with bigger grains and this leads to low tensile strength since bigger grains can easily move dislocations, hence making the material soft.

Conclusions

The weld joints welded at a welding current of 5 to 7.5 A, SOD of 2 to 4 mm and welding speed of 120 to 240 mm/min at the same plasma and shielding gas flow rate of 0.6 Lpm and 6 Lpm did not show any surface defects. The mathematical models development could be effectively done using a three level three factor design matrix, which is based on the face centered central composite design technique. The created models can be predictively utilized to anticipate the tensile strength and microhardness of MPAW weld joints over the range of parameters. The final tensile strength, and microhardness are the highest at the welding parameters i.e., welding current 6.25 A, SOD 3 mm and speed 180 mm/min 527.5 Mpa and 191.85 HV respectively. It was noted that the higher the cooling

10.48047/jocaaa.2022.30.02.78

rate (265.5K/s) the finer the grain structures were formed whereas the slower the cooling rate (80K/s) the more time the alloying elements such as chromium to segregate and cluster giving it more chances to form delta ferrite. The faster the cooling rate (265.5K/s) the higher the microhardness and tensile strength and the slower the cooling rate (80K/s) the lower is the microhardness and tensile strength.

References

1. D. Deng, H. Murakawa, Prediction of welding distortion and residual stress in a thin plate butt-welded joint. J. Computat. Materials Science. 43(2), (353-365) (2008).

2. Blondeau, R. Metallurgy and Mechanics of Welding Process and Industrial Applications. Wiley-ISTE, 2008.

3. A. Sahoo, S. Tripathy, Development in plasma arc welding process: A review. Materials Today: Proceedings. 41(2), 363-368 (2021).

4. Golański, Dariusz, et al., Advanced Applications of Microplasma Welding. BiuletynInstytutuSpawalnictwa w Gliwicach. 62(5), 53-63. (2018).

5. Batool, Sadaf, et al., Analysis of weld characteristics of micro-plasma arc welding and tungsten inert gas welding of thin stainless steel (304L) sheet. Proceedings of the Institution of Mechanical Engineers, Part L: Journal of Materials: Design and Applications 230(6), 1005-1017. (2016).

6. H. Vashishtha, R.V. Taiwade, S. Sharma, A.P. Patil, Effect of welding processes on microstructural and mechanical properties of dissimilar weldments between conventional austenitic and high nitrogen austenitic stainless steels. J. Manuf. Process. 25, 49–59 (2017).

10.48047/jocaaa.2022.30.02.78

7. M.F. McGuire, Austenitic Stainless Steels, Encyclopaedia of Materials: Science and Technology (Second Edition), 406-410 (2001).

8. G. Shit, M.V. Kuppusamy, S. Ningshen, Corrosion resistance behavior of GTAW welded AISI type 304L stainless steel. Trans. Indian Inst. Met. 72, 2981 (2019).

9. P. Vasantharaja, M. Vasudevan, V. Maduraimuthu, Effect of arc welding processes on the weld attributes of type 316LN stainless steel weld joint. Trans. Indian Inst. Met. 71(1), 127–137 (2018).

10. H.M. Soltani, M. Tayebi, Comparative study of AISI 304L to AISI 316L stainless steels joints by TIG and Nd:YAG laser welding. J. Alloys Compd. 767, 112–121 (2018).

11. R. Singh, R.S. Slathia, Effect of cryogenic treatment on sensitization of 304 stainless steel in TIG welding. J. Inst. Eng. India Ser. C 97(2), 127–130 (2016).

12. M. Azadi Moghaddam and F. Kolahan, Optimization of A-TIG welding process using simulated annealing algorithm, Journal of Advanced Manufacturing Systems. 19(4), 869-891 (2020).

13. K. Siva Prasad, Tarun Bayya, Effect of Pulsed Current Micro Plasma Arc parameters on weld bead geometry of AISI 316Ti Austenitic Stainless Steel, Journal of Mechanical and Mechanics Engineering. 3(1), 56-65 (2017).

14. Li X, Liang J, Shi T, Yang D, et al. , Tribological behaviors of vacuum hot-pressed ceramic composites with enhanced cyclic oxidation and corrosion resistance. Ceram Int. 46(9), 11–20 (2020).

10.48047/jocaaa.2022.30.02.78

15. Karimzadeh F, Salehi M, et. al., Effect of MPAW process parameters on grain growth and porosity distribution of thin sheet Ti6Al4V alloy Weldment. Mater Manuf Process. 20(2):205–219 (2005).

16. E. F. Gorman: Weld. J., 48, (7), 547 – 556 (1969).

17. R. L. OBRIEN: Weld. Res. Counc. Bull. 131, 1 – 37 (1968).

18. W. Lucas: in 'TIG and plasma welding', Cambridge, UK, Abington Publishing. 1st edn., 80 – 108 (1990).

19. K. H. Tseng, S. T. Hsieh et. al., Effect of process parameters of micro-plasma arc welding on morphology and quality in stainless steel edge joint welds, Sci. and Tech. of Welding and Joining 8(6), 423-430 (2003).

20.S. Wang, J. Goldak et. al, Simulation on the thermal cycle of a welding process by space-time convection-diffusion finite element analysis, Int. J. Therm. Sci. 48 (5), 936–947 (2009).

21. C.S. Wu, Q.X. Hu, J.Q. Gao, An adaptive heat source model for finite-element analysis of keyhole plasma arc welding, Comput. Mater. Sci. 46 (1), 167– 172 (2009).

22. Benjamin Das, Y. Nirsanametla et. al., An investigation on heat transfer analysis of Micro-Plasma arc welds using finite element method, Materials Today: Proceedings 62 4249–4253 (2022).

23. Baruah, M. and Bag, S.,Characteristic difference of thermo-mechanical behaviour in plasma microwelding of steels. Welding in the World, 61, 857-871 (2017).

10.48047/jocaaa.2022.30.02.78

24. Zhao H, Zhang G et. al., A 3D dynamic analysis of thermal behavior during single-pass multi-layer weld-based rapid prototyping. J Mater Process Tech. 211(3), 488–495 (2011).

25. SwagatDwibed&Swarup Bag, Development of Micro-plasma Arc Welding System for Different Thickness Dissimilar Austenitic Stainless Steels. J. Inst. Eng. India Ser. C 102(3), 657-671 (2021).

26. S. Dwibedi and S. Bag, Influence of process parameters on microstructural evolution, solidification mode, and impact strength in joining of stainless steel thin sheets. Advances in Materials and Processing Technologies. 8(3), 1089–1104 (2022).

27. S. Dwibedi and S. Bag. Development of Micro-plasma Arc Welding System for Different Thickness Dissimilar Austenitic Stainless Steels. Journal of The Institution of Engineers (India): Series C. 102(3), 657–671 (2021).

28. Goyal, Ashish, et al., Experimental investigation to analyze the mechanical and microstructure properties of 310 SS performed by TIG welding. Advances in Materials Science and Engineering 2022 (2022).

29. Ghusoon R. et. al., The effect of fiber laser parameters on microhardness and microstructure of duplex stainless steel. MATEC Web of Conferences 90, 01024 (2017).